

The Effect of Silver Nanoparticles on the Photodetecting Properties of the TiO₂/Graphene Oxide Nanocomposite

E. V. Seliverstova^{a,*}, N. Kh. Ibrayev^{a,**}, and A. Zh. Zhumabekov^a

^a Institute of Molecular Nanophotonics, Buketov Karaganda State University, Karaganda, 100028 Kazakhstan

*e-mail: genia_sv@mail.ru

**e-mail: niazibrayev@mail.ru

Received April 21, 2020; revised April 30, 2020; accepted May 20, 2020

Abstract—The effect of silver nanoparticles on the optoelectronic and photoelectric properties of a nanocomposite material based on graphene oxide (GO) and TiO₂ was studied. It was shown by electron microscopy and Raman spectroscopy that during hydrothermal synthesis, a TiO₂–GO nanocomposite material is formed as a result of the hydrothermal synthesis, as shown by electron microscopy and Raman spectroscopy. The absorption spectrum of the nanocomposite is shifted to the long-wavelength region relative to the absorption spectrum of TiO₂. The current–voltage characteristics of photodetectors based on TiO₂–GO nanocomposite films without Ag nanoparticles and TiO₂–GO nanocomposite films with addition of Ag nanoparticles increase relative to the current–voltage characteristics of pure titanium dioxide by factors of 2 and 7.5, respectively. The optoelectronic parameters of the relevant devices also increase, which is associated with an increase in the mobility of charge carriers in nanocomposite films.

Keywords: nanocomposite, graphene oxide, titanium dioxide, photodetector, Ag nanoparticles

DOI: 10.1134/S0030400X20090192

INTRODUCTION

Transition metal oxides offer great opportunities for the optoelectronic applications for which high sensitivity to ultraviolet radiation is required. Ultraviolet photodetectors can be used for both civilian and military purposes, including biological and chemical analyses, as well as environmental monitoring [1, 2]. Ultraviolet photodetectors are usually made of wide-gap semiconductor materials, such as TiO₂ [3–5], ZnO [6], and ZnS [7].

Titanium dioxide TiO₂ is among the most studied semiconductors due to the high promise of its application in photocatalysis, photovoltaic cells, and gas sensors [8–10]. Titanium dioxide with a band gap of 3.2 eV is sensitive to light with wavelengths below 380 nm. This allows one to use it in the manufacture of UV-range photodetectors. Many authors have shown that the doping of TiO₂ with carbon nanostructures gives rise to increases in both the sensitivity and performance of devices based on it. With this aim, carbon materials of various nature, such as activated carbon, carbon black, carbon fibers, and carbon nanotubes, were studied [11, 12].

However, the most promising materials for practical applications are, in our opinion, graphene oxide (GO) and its derivatives [11–16]. In [17], we demonstrated that the addition of GO and reduced GO to TiO₂ leads to a nearly ten-fold increase in its photocat-

alytic activity, which is the result of an increase in the adsorption characteristics, and an improvement in the photoelectric parameters and light harvesting efficiency of the synthesized nanocomposites.

Currently, graphene and titanium dioxide are normally used in photodetecting devices in the form of layered structures or in combination with semiconductor nanostructures (nanorods, nanospheres, and nanosized tracks) [18–20]. Meanwhile, studies devoted to photodetectors based on TiO₂ nanocomposites and graphene oxide distributed over the semiconductor volume are nearly absent. This paper presents the results of a study of the optoelectronic and photoelectric parameters of such a photodetector. It is shown that widely available and easy-to-handle graphene oxide makes it possible to significantly increase the performance of TiO₂-based UV detectors.

The incorporation of plasmon silver nanoparticles into nanocomposite layers allows one to improve the photodetecting properties of the synthesized material. It is believed that the inclusion of metal plasmon nanostructures into graphene enhances the light–substance interaction [21, 22]. Such nanostructures were used in surface-enhanced Raman spectroscopy (SERS) and single-molecule spectroscopy, and to improve photodetection, photovoltaics, and light-emitting devices.

It was shown in [23–29] that the presence of plasmonic Ag or Au nanoparticles enhances both the photocatalytic and photovoltaic characteristics of TiO₂–graphene nanocomposites. Moreover, the optimization of photoreactions in the presence of plasmons in semiconductors is ascribed to an increase in the generation and separation of electron–hole pairs (EHPs), as well as to broadening the range of the photoactivity of the material in the direction of the visible light region [26–29]. We also attempted to use the plasmon effect of silver nanoparticles to increase the optoelectronic parameters of detectors based on a TiO₂–GO nanocomposite.

EXPERIMENTAL

The nanocomposite based on TiO₂ and GO was synthesized using the hydrothermal method by the procedure described in [17, 30]. Graphene oxide (SLGO, Cheaptubes) and TiO₂ ($d > 21$ nm, anatase 99.7%, Sigma Aldrich), deionized water (water treatment system AquaMax), and ethanol (anhydrous) were used in the synthesis. The concentration of GO in the nanocomposite was 5 wt % with respect to TiO₂, since it was previously shown that the largest increase in the charge-transport parameters and photocatalytic activity of the synthesized nanocomposite is recorded with this ratio of components [17].

The surface morphology and microstructure of the obtained composite were studied on a Mira 3MLU scanning electron microscope (SEM) from Tescan and a JEM-2100F transmission electron microscope (TEM) with an accelerating voltage of 120 kV from Jeol.

Nanoparticles (NPs) of Ag in ethanol were obtained by ablation of a silver target with the second harmonic of a solid-state Nd : YAG laser (SOLAR LQ215, $\lambda_{\text{gen}} = 532$ nm, $\tau = 7$ ns, and $\nu = 20$ Hz) in accordance with the procedure described in [31]. According to the SEM data, they have a spherical shape. The concentration of silver NPs in the working solution was $C_{\text{Ag}} = 1 \times 10^{-10}$ mol/L. The average diameter of the NPs was determined by the dynamic light scattering method on a Nanosizer 90S analyzer (Malvern) and was equal to 31 ± 7 nm.

Films based on TiO₂ or TiO₂–GO nanocomposite were prepared from a paste prepared by continuously mixing 150 mg of a TiO₂ or TiO₂–GO powder with 1 mL of ethanol for 24 h. Nanocomposite films with plasmon NPs were obtained by adding the required amounts of solutions of Ag NPs to the prepared paste and additionally mixing them for 24 h. The concentrations of Ag NPs in such pastes were equal to 10^{-11} , 10^{-12} , or 10^{-13} mol/L.

The prepared paste was applied to the surface of the substrates by the spin-coating method at a rotation speed of 2000 rpm. According to SEM, the average

film thickness was 4.2 μm . After deposition, the film was annealed in an Ar atmosphere for 2 h at a temperature of 450°C. The films for optical measurements were formed on quartz substrates.

To assemble a photodetector, glass with a conductive layer of fluorinated tin oxide (FTO, about 7 Ω/sq) from Sigma Aldrich was used. On the surface of the substrates, tracks of the intradigital type were carved (Fig. 1) using a BLS0503MM laser scriber (Bodor). The distance between the tracks was 1.5 mm, and the length of the tracks was 10 mm. SEM measurements showed that tracks with a width of 250–280 μm are formed during scribing and a film is formed on top of the channel when applying the paste.

A Confotec MR520 microscope (Sol Instruments) with laser excitation at a wavelength of 632.8 nm was used to record the Raman spectra of the nanocomposite material.

The current–voltage characteristics (CVC) of the prepared samples were measured using an Elins P-20X potentiostat/galvanostat (Elins) under irradiation of the samples with light of a xenon lamp with a power of 35 mW/cm².

To study the response time of the samples, a setup with the circuit shown in Fig. 2 and a LQ215 pulsed laser (SOLAR) with a generator of the third harmonic with $\lambda_{\text{gen}} = 355$ nm and a pulse duration of 7 ns were used.

Upon irradiation of the detector, the photoelectric voltage signal of the sample was applied to a Bordo-211 digital oscilloscope with a maximum sensitivity of 10 mV/div. Thereby, a constant voltage of 9 V was applied to the sample. The measurements were carried out in the excitation mode with single pulses. To synchronize the start of the oscilloscope sweep with the start of the exciting light pulse and to ensure the specified delay time, the Arduino-based software and hardware were used. The value of the RC constant of the measuring circuit did not exceed 1 μs , and the experimentally selected delay time was 100 μs .

RESULTS AND DISCUSSION

The data shown in Fig. 3 were obtained in the study of the microstructure of the nanocomposite material and its starting components. As can be seen from Fig. 3, the nanoparticles in a titanium dioxide sample are aggregated. Interparticle pores can be distinguished in the image. Graphene oxide is present in the form of layered flakes, in which the sheets are prone to the formation of wrinkles and folds due to the presence of oxygen-containing groups in its structure. Thin GO sheets distributed over the surface of TiO₂ nanoparticles and between them are clearly distinguishable in the nanocomposite, as is seen in TEM images. It is evident that TiO₂ particles after the hydrothermal synthesis are not just located on the surface of GO, but are enveloped by them. This will allow TiO₂ particles to

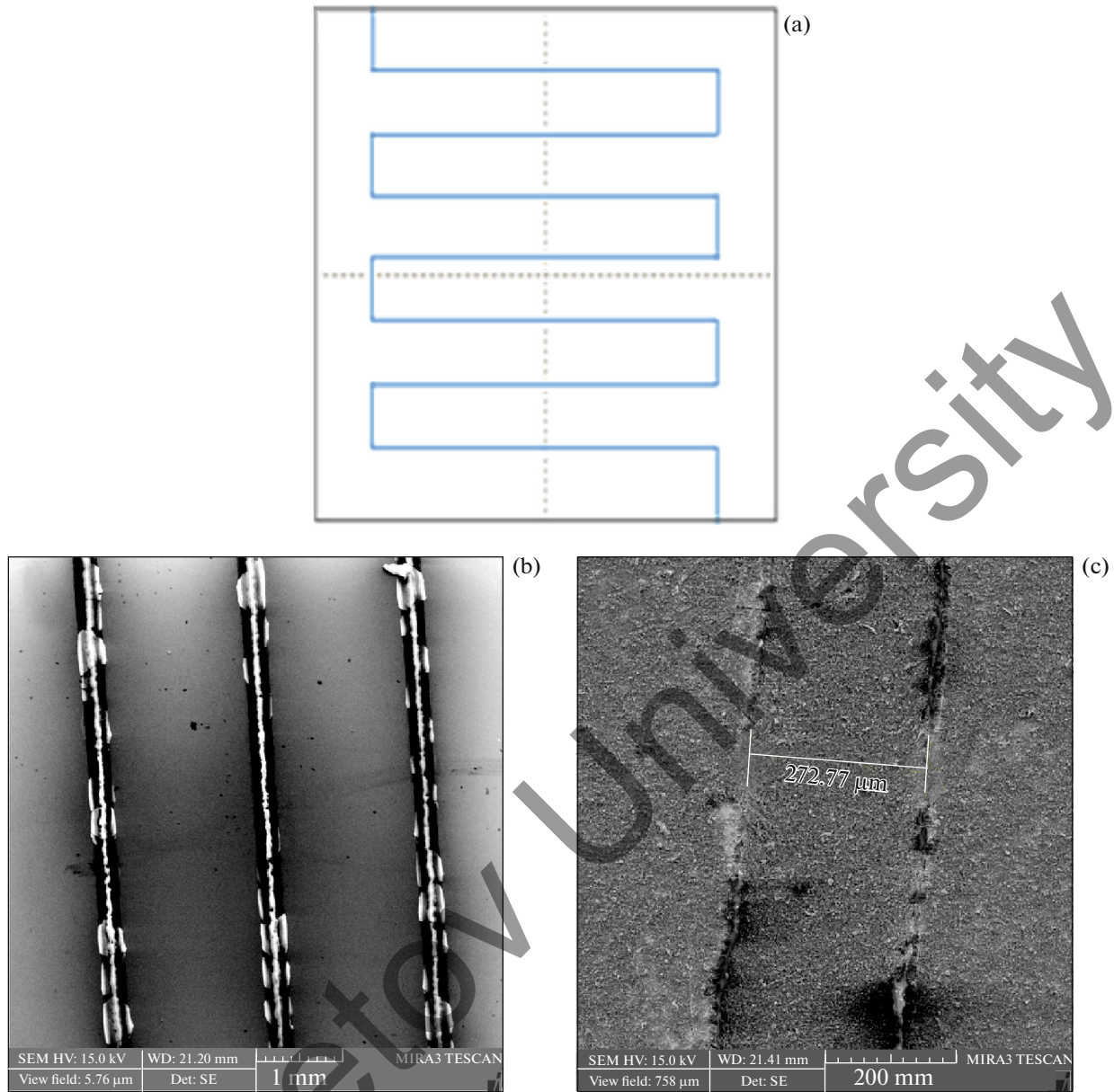


Fig. 1. (a) Scheme of tracks and (b, c) the SEM image of tracks on the FTO surface and (c) the SEM image of the TiO₂ film on the track surface.

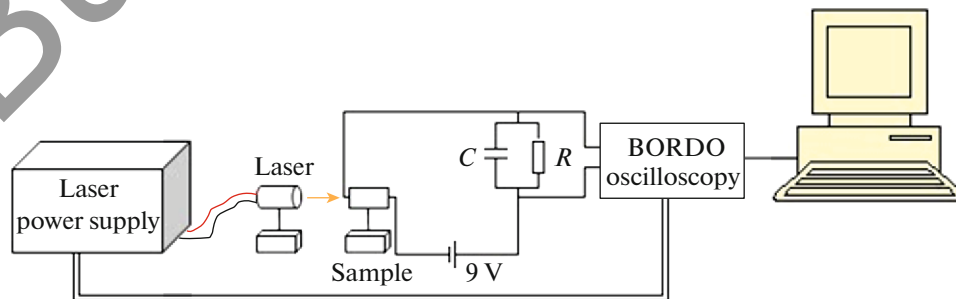


Fig. 2. Block diagram of an experimental setup for studying the response time.

Table 1. Optoelectronic parameters of films based on TiO₂, TiO₂–GO and nanocomposites with addition of Ag NPs

Sample	I_{ph} , μA at +30 V	R , A/W	D^* , Jones
TiO ₂	1.10	31.0×10^{-6}	6.3×10^7
TiO ₂ –GO	1.98	56.0×10^{-6}	6.2×10^7
TiO ₂ –GO + Ag (10^{-13})	8.30	237.0×10^{-6}	12.0×10^7
TiO ₂ –GO + Ag (10^{-12})	0.78	22.3×10^{-6}	6.4×10^7
TiO ₂ –GO + Ag (10^{-11})	0.40	11.4×10^{-6}	0.1×10^7

inject their photogenerated electrons into the GO sheets under the influence of light, ensuring their efficient transport to the FTO layer and further detection [30].

Silver nanoparticles are practically indistinguishable in the images of nanocomposite films due to their low concentration, therefore their presence was confirmed by energy dispersive X-ray analysis (EDX, Fig. 3f).

We also measured the Raman spectra of the samples under study (Fig. 4). Titanium dioxide with the anatase structure has six Raman active peaks in the vibrational spectrum [30, 32]. Among them, there are three E_g peaks at about 150, 180, and 630 cm⁻¹, two B_{1g} peaks at 395 and 505 cm⁻¹, and an A_{1g} peak at 481 cm⁻¹. The spectrum GO contains the following two characteristic bands: the D band at about 1350 cm⁻¹, which characterizes the degree of imperfection of graphene; and the G band at about 1590 cm⁻¹. The I_D/I_G intensity ratio is 1.2. The Raman spectra of the nanocomposite are a combination of the spectra of individual components. The I_D/I_G intensity ratio in the nanocomposite material is 1.03. A decrease in this parameter indicates the occurrence of graphene oxide reduction during the synthesis process, during which carbon sp² domains can be formed and the number of oxygen-containing groups can decrease [33].

Measurements of the optical properties of the studied films showed that a bathochromic shift of the edge of the TiO₂ absorption band is observed in the presence of GO. In the absorption spectrum of a nanocomposite with Ag NPs, a very weak maximum of about 420 nm is identified. Moreover, there are no such changes in the spectra of the initial components. In particular, the edge of the absorption band of titanium dioxide is located at 380 nm, and a maximum at about 230 nm is noticeable in the absorption spectrum of GO [34, 35]. It is known that the absorption band at 230 nm is caused by the ππ* transitions between electronic orbitals of C–C aromatic bonds. The long-wavelength shift of the edge of the absorption band of the nanocomposite is associated with a change in the band gap of such a material in comparison with pure

TiO₂ [30]. This can lead to a higher light absorbing ability of the TiO₂–GO nanocomposite.

The current–voltage characteristics of the measured samples, as well as some of their optoelectronic parameters, are shown in Fig. 5a and Table 1. The current–voltage characteristics were measured both at a positive voltage bias (up to +30 V) and at negative values of up to –5 V. The I(U) dependence curves are nonlinear in behavior. Moreover, large current values are recorded even in the absence of illumination of the samples.

With photoirradiation of the TiO₂ samples, a maximum current value of 2 μA was recorded. The values of generated photocurrent I_{ph} of the detector, which are calculated from the difference between the I values under dark and illuminated conditions are shown in Table 1. As can be seen from Fig. 5a, the I_{ph} values for films based on the TiO₂–GO composition are almost three-fold higher; however, the I_{ph} value of such a photodetector increases only by a factor of 1.8 due to the presence of a large dark current when compared to pure TiO₂. For photodetectors with plasmon NPs, the photocurrent values increased only with an Ag concentration of 10⁻¹³ mol/L. It can be seen that the dark and light currents increased almost proportionally. Hereinafter, this concentration of silver NPs will be understood when mentioning the parameters of the TiO₂–GO + Ag photodetector.

The enhancement of photocurrent I_{ph} of the detector based on a three-component film was 4.2-fold of that for TiO₂–GO films and 7.5-fold of that for pure titanium dioxide. With further addition of Ag NPs to the nanocomposite film, a decrease in the I_{ph} value is recorded, which is associated with small values of both the dark and light currents. In particular, the I_{dark} values for silver concentrations from 10⁻¹³ to 10⁻¹¹ mol/L were 12.14, 0.38, and 0.78 μA, respectively. As can be seen, there is a nonlinear dependence of the I_{dark} value on the concentration of Ag NPs. However, it is known that the drift current density is directly proportional to the conductivity of the semiconductor. Therefore, we can conclude that this parameter increases at low concentrations of Ag NPs. At the same time, the conductivity also depends on the drift velocity or mobility of charge carriers.

It is still difficult to conclude on the basis of obtained data, which one of the mechanisms contributes more to an increase in the photocurrent of the detector based on a nanocomposite with the addition of plasmon NPs; therefore, the kinetics of generation and transport of charge carriers in the prepared photodetectors were further studied (Fig. 5b). As can be seen from the kinetic data, the time of photovoltage growth in all films is much shorter than the decay time. The complete kinetics of voltage decay in the studied films can be described using the biexponential equation. Characteristic times, such as grow time t_{grow} and

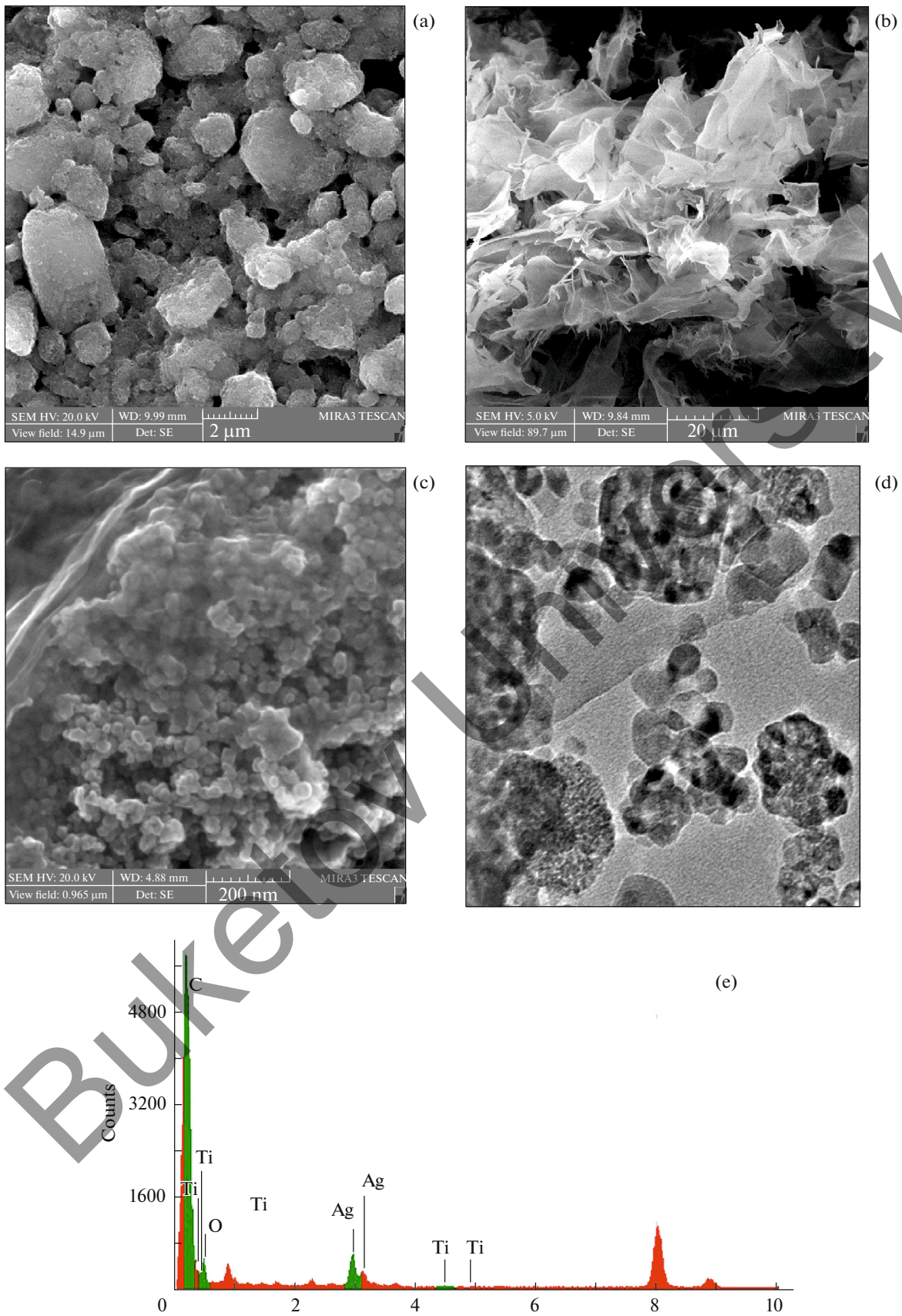


Fig. 3. (a–c) SEM and (d) TEM images of the (a) TiO_2 , (b) GO nanocomposites, and (c, d) TiO_2 -GO nanocomposites, and (e) the EDX analysis of TiO_2 -GO with Ag NPs.

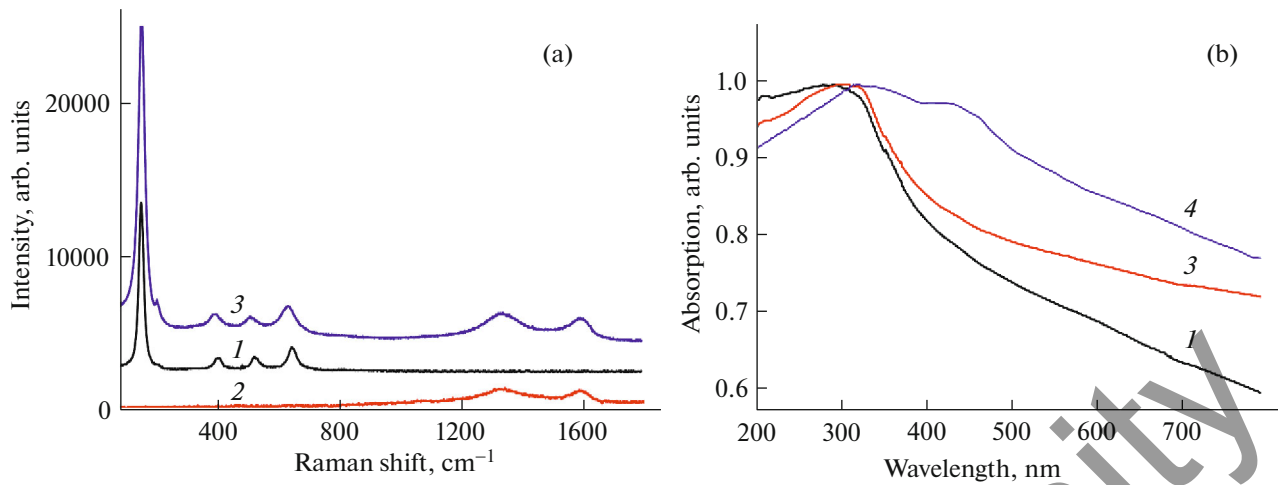


Fig. 4. (a) Raman and (b) absorption spectra of films of (1) TiO_2 , (2) GO, (3) TiO_2 -GO, and (4) TiO_2 -GO + Ag with $C_{\text{Ag}} = 10^{-11}$ mol/L.

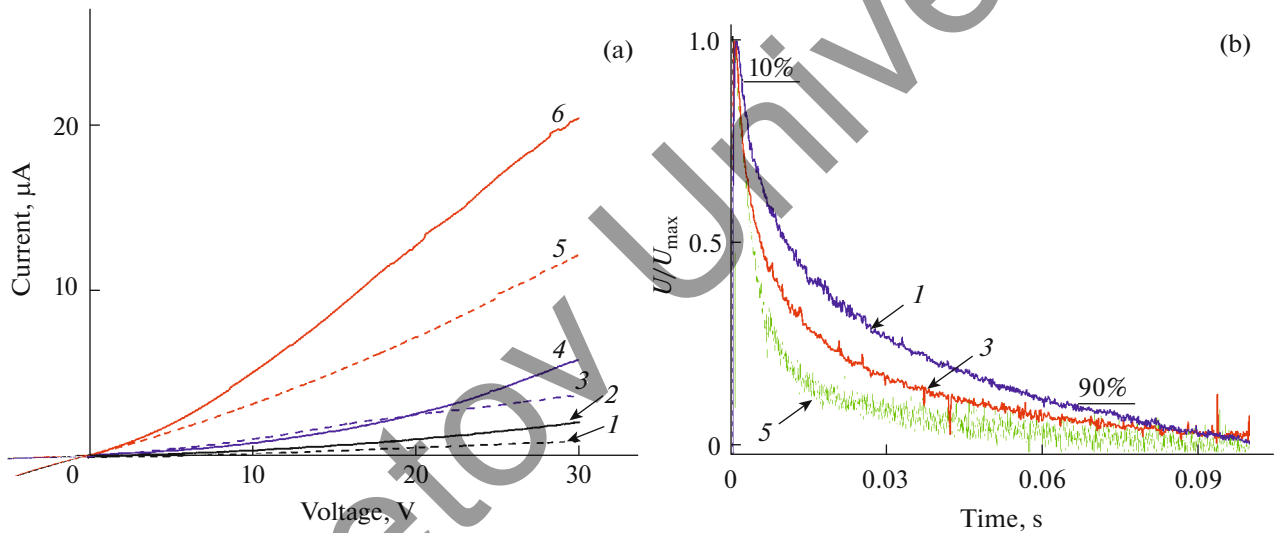


Fig. 5. (a) Dark (1, 3, 5) and light (2, 4, 6) current–voltage characteristics and (b) the kinetics of generation and decay of charge carriers in films based on (1, 2) TiO_2 , (3, 4) TiO_2 -GO, and (5, 6) TiO_2 -GO + Ag with $C_{\text{Ag}} = 10^{-13}$ mol/L.

charge carrier lifetimes t_1 and t_2 , were determined from the kinetic data (Table 2).

As can be seen from Fig. 5b, the times of photoconductivity relaxation in a TiO_2 -based detector are longer than that for nanocomposite samples. A decrease in the growth time of voltage kinetics by 46% was recorded for photodetectors with GO compared to pure TiO_2 , and the charge carrier lifetimes also decreased. It can be concluded that the generation and separation of charge carriers in the TiO_2 -GO samples occurs in less time. In the presence of Ag NPs, a fur-

ther decrease in both the t_{grow} values and the t_1 and t_2 lifetimes occurs.

Next, transit time t_{tr} that corresponds to the time point at which the center of gravity of the drifting package of charge carriers leaves the sample and the mobility of charge carriers were determined by the technique proposed in [36]. For this, a double logarithmic plot of the time dependence of the photogeneration voltage was constructed. The inflection point of the curve was taken as time t_{tr} required for the center of gravity of the drift packet of charge carriers to leave the sample. This time was 5.9 μs for the TiO_2 samples, and

5.1 and 2.5 μs for the $\text{TiO}_2\text{-GO}$ and $\text{TiO}_2\text{-GO} + \text{Ag}$ samples, respectively. Mobility μ_d of charge carriers was estimated using the following expression:

$$\mu_d = \frac{d}{t_{tr}E},$$

where d is the film thickness, and E is the voltage applied to the sample (9 V).

The μ_d value for a titanium dioxide film was 7.9×10^{-2} m/(V s), whereas this value for a film based on $\text{TiO}_2\text{-GO}$ increased to 9.1×10^{-2} m/(V s) or by a factor of 1.15. With the addition of Ag NPs, it increased further by a factor of 2.35 or to 18.6×10^{-2} m/(V s). Thus, it can be concluded that the mobility of charge carriers in photodetectors with graphene oxide increases. A further increase in the μ_d value was also observed upon the addition of Ag NPs to semiconductor films.

When evaluating the optoelectronic parameters of the prepared samples, we assessed sensitivity R , detectivity D^* , and the time of photoresponse of the detectors. Sensitivity R of the photodetectors was calculated using the formula $R = I_{ph}/P$, where P is the power of the incident radiation. As is seen from Table 1, the sensitivity of composite films is 1.8 times higher than that of pure TiO_2 films. The best photodetector sensitivity is observed for films with Ag NPs added in the same concentration as in the case of measuring the photocurrent values. The sensitivity of such a film is about 0.24 mA/W, which is 4.2 times higher than that of films without the addition of NPs.

Next, detectivity D^* of the prepared samples was estimated, which determines the ability of the device to detect weak light signals which and can be found [37, 38] from the following expression:

$$D^* = \frac{RA^{1/2}}{\sqrt{2eI_{dark}}},$$

where R is the sensitivity of the film, A is the illuminated area of the sample, e is the absolute value of the electron charge, and I_{dark} is the dark current. The values obtained for both pure TiO_2 and $\text{TiO}_2\text{-GO}$ are about 6×10^7 Jones. With a minimum content of Ag NPs in the film, the detecting ability of the photodetector increased by almost a factor of 2. This fact indicates that an increase in this parameter is associated with a substantial increase in the generated photocurrent despite the significant I_{dark} value, as is observed in a system without plasmons.

Comparing the obtained R and D^* values of the photocurrent to the data published by other authors [39, 40], it can be noted that the performance of $\text{TiO}_2\text{-GO}$ films is not inferior to that of samples based on pure graphene and the generated I_{ph} values are even superior.

The time of detector photoresponse (or turn-on time) was determined from the kinetic data as a time

Table 2. Time characteristics of films based on TiO_2 , $\text{TiO}_2\text{-GO}$ and nanocomposites with addition of Ag NPs

Sample	t_{grow} , s	t_1 , s	t_2 , s
TiO_2	40.5×10^{-3}	0.95	1.9
$\text{TiO}_2\text{-GO}$	27.7×10^{-3}	0.45	1.84
$\text{TiO}_2\text{-GO} + \text{Ag} (10^{-13})$	0.7×10^{-3}	0.25×10^{-3}	2.4×10^{-3}
$\text{TiO}_2\text{-GO} + \text{Ag} (10^{-12})$	3.2×10^{-6}	0.14×10^{-3}	1.5×10^{-3}
$\text{TiO}_2\text{-GO} + \text{Ag} (10^{-11})$	49.0×10^{-6}	0.85×10^{-3}	3.7×10^{-3}

period during which the photovoltage or current value varies from 10 to 90% of its maximum value (Fig. 5b), according to the methodology described in [37, 40]. For the TiO_2 sample, this parameter is equal to 58 μs . For films with GO and GO + Ag, the photoresponse time decreases to 39 and 9.5 μs , respectively. Thus, the turn-on time of a semiconductor detector based on TiO_2 can be shortened by a factor of about 1.5 or 6.1 with the addition of GO or GO and plasmon NPs, respectively. It should be noted that the photoresponse time obtained in this study is shorter than that for a TiO_2 detector with Ni electrodes (11.43 s) [41], as well as than that for detectors based on $\text{TiO}_2\text{-graphene}$ (1.1 s) [37] and graphene-reduced GO layered structures (114 μs) [42].

As determined from the dark characteristics with respect to the I_{1V}/I_{-1V} ratio [40], the rectification factors of the photodetector were 0.92, 3.03, and 0.85 for films based on pure TiO_2 , $\text{TiO}_2\text{-GO}$, and $\text{TiO}_2\text{-GO} + \text{Ag}$, respectively. It can be seen that the studied detectors exhibit weak rectifying properties.

As indicated in [17, 38], the improvement of the photoelectric parameters of $\text{TiO}_2\text{-GO}$ films is a result of an improvement in the charge-transport characteristics of the synthesized films, as well as a result of accelerating the process of charge separation in the film. In this case, graphene sheets serve as transport channels for transferring charge carriers to the counter electrode. In fact, it was found from the photodetector resistance estimated according to Ohm's law using the voltages determined on the basis of the kinetic data that the resistance is 154.5 Ω for the TiO_2 -based detector and 32 Ω for the $\text{TiO}_2\text{-GO}$ films. With the addition of Ag NPs, the resistance of the samples decreased to 20 Ω .

Thus, it can be seen that the addition of GO to TiO_2 allows one to several times reduce the resistance values of the semiconductor film, which agrees with the data published in [17, 37] about achieving this by transferring electrons through the sheets of GO. In the presence of Ag NPs, an additional decrease in the nanocomposite resistance to electron transport is observed. An increase in the photoconductivity of titanium dioxide films in the presence of GO is also confirmed

by an increase in the mobility of charge carriers in nanocomposites with and without Ag NPs.

CONCLUSIONS

The performed studies have shown that the current and optoelectronic parameters of the photodetector can be improved using a nanocomposite material based on TiO₂ and GO. These parameters can be enhanced by adding Ag NPs.

A study of the current–voltage characteristics of the photodetector has shown that the photocurrent of the device increases by a factor of 1.8 in the presence of graphene oxide. For photodetectors with plasmon NPs, the photocurrent values increase only with an Ag concentration of 10⁻¹³ mol/L. In this case, an increase in the photocurrent for the three-component film is 4.2 times higher than that for the TiO₂–GO films and 7.5 times higher than that for pure titanium dioxide. Sensitivity *R* and the specific detecting ability of photodetectors with plasmon NPs also increase.

It is shown that an increase in the photocurrent of the detector is mainly associated with an increase in the mobility of charge carriers, as follows from the photoconductivity kinetics. As can be noted from comparison of the mobilities of charge carriers in TiO₂ (about 10⁻⁵ cm²/(V s) [43]) and graphene (2.5 × 10⁵ cm²/(V s) [44]), the charge transport properties of the nanocomposite are improved owing to the high charge mobility in the graphene component.

In addition, the resistance to electron transport decreases when both GO and Ag NPs are added to the synthesized films, which indeed indicates an increase in the charge-transport parameters of the synthesized films. This is consistent with our previous results for a nanocomposite based on TiO₂ and reduced graphene oxide [30].

The enhancement of the photocurrent in hybrid devices based on graphene and silver nanoparticles can be explained by both an increase in the electric field near Ag NPs [45, 46] and light scattering by silver nanoparticles. This field can increase the absorption of the nanocomposite in the visible region of the spectrum [46] and also leads to an increase in the mobility of charge carriers inside the graphene component of the nanocomposite [47].

FUNDING

This work was supported by the Ministry of Education and Science of the Republic of Kazakhstan within research grants AP05132443 and BR05236691.

ACKNOWLEDGMENTS

We are grateful to Dr. D.A. Afanas'ev for consultations in conducting pulse measurements and discussing the results.

CONFLICT OF INTEREST

The authors declare that they have no conflicts of interest.

REFERENCES

1. X. Yu, Z. Zhao, J. Zhang, W. Guo, J. Qiu, D. Li, Z. Li, X. Mou, L. Li, A. Li, and H. Liu, *Small* **12**, 2759 (2011). <https://doi.org/10.1002/sml.201503388>
2. M. Peng, Y. Liu, A. Yu, Y. Zhang, C. Liu, J. Liu, W. Wu, K. Zhang, X. Shi, J. Kou, J. Zhai, and Z. L. Wang, *ACS Nano* **10**, 1572 (2016). <https://doi.org/10.1021/acs.nano.5b07217>
3. Q. Wang, J. J. Li, and C. Z. Gu, *J. Phys. Chem. C* **116**, 16864 (2012). <https://doi.org/10.1021/jp304193z>
4. Y. Han, G. Wu, H. Li, M. Wang, and H. Chen, *Nanotechnology* **21**, 185708 (2010). <https://doi.org/10.1088/0957-4484/21/18/185708>
5. L. B. Wang, W. Y. Yang, H. N. Chong, L. Wang, F. M. Gao, L. H. Tian, and Z. B. Yang, *RSC Adv.* **5**, 52388 (2015). <https://doi.org/10.1039/C5RA05861A>
6. H. L. Xue, X. Z. Kong, Z. R. Liu, C. X. Liu, J. R. Zhou, W. Y. Chen, S. P. Ruan, and Q. T. Xu, *Appl. Phys. Lett.* **90**, 201118 (2007). <https://doi.org/10.1063/1.2741128>
7. Y. Liang, H. Liang, X. D. Xiao, and S. K. Hark, *J. Mater. Chem.* **22**, 1199 (2012). <https://doi.org/10.1039/c1jm13903g>
8. H. D. Jang, S. K. Kim, H. Chang, E. H. Jo, K. M. Roh, J. H. Choi, and J. W. Choi, *Aerosol Sci. Technol.* **49**, 538 (2015). <https://doi.org/10.1080/02786826.2015.1050086>
9. A. Molina-Mendoza, A. Moya, R. Frisenda, S. A. Svaitek, P. Gant, S. Gonzalez-Abad, E. Antolin, N. Agrait, G. R. Bollinger, D. Perez de Lara, J. Vilatela, and A. Castellanos-Gomez, *J. Mater. Chem. C* **4**, 10707 (2016). <https://doi.org/10.1039/C6TC02344D>
10. N. Ibrayev, E. Seliverstova, and G. Omarova, *Mater. Today: Proc.* **25**, 39 (2020). <https://doi.org/10.1016/j.matpr.2019.11.016>
11. R. Leary and A. Westwood, *Carbon* **49**, 741 (2011). <https://doi.org/10.1016/j.carbon.2010.10.010>
12. N. Takeda, N. Iwata, T. Torimoto, and H. Yoneyama, *J. Catal.* **177**, 240 (1998). <https://doi.org/10.1006/jcat.1998.2117>
13. Y. H. Ng, I. V. Lightcap, K. Goodwin, M. Matsumura, and P. V. Kamat, *J. Phys. Chem. Lett.* **1**, 2222 (2010). <https://doi.org/10.1021/jz100728z>
14. Q. Li, B. D. Guo, J. G. Yu, J. R. Ran, B. H. Zhang, and H. J. Yan, *J. Am. Chem. Soc.* **133**, 10878 (2011). <https://doi.org/10.1021/ja2025454>
15. H. Zhang, X. J. Lv, Y. M. Li, Y. Wang, and J. H. Li, *ACS Nano* **4**, 380 (2010). <https://doi.org/10.1021/nn901221k>
16. Y. Zhou, Q. L. Bao, L. A. L. Tang, Y. L. Zhang, and K. P. Loh, *Chem. Mater.* **21**, 2950 (2009). <https://doi.org/10.1021/cm9006603>

17. N. Ibrayev, A. Zhumabekov, S. Ghyngazov, and E. Ly-senko, *Mater. Res. Express* **6**, 125036 (2019).
<https://doi.org/10.1088/2053-1591/ab51a3>
18. D. Zhang, F. Jing, F. Gao, L. Shen, D. Sun, J. Zhou, Y. Chen, and S. Ruan, *RSC Adv.* **5**, 83795 (2015).
<https://doi.org/10.1039/C5RA17023K>
19. X. Yu, Y. Li, X. Hu, D. Zhang, Y. Tao, Z. Liu, Y. He, Azimul Md. Haque, Zh. Liu, T. Wu, and Q. L. Wang, *Nat. Commun.* **9**, 4299 (2018).
<https://doi.org/10.1038/s41467-018-06776-z>
20. M. Zh. Wang, F. X. Liang, B. Nie, L. H. Zeng, L. Xia Zheng, P. Lv, Yong Qiang Yu, Ch. Xie, Ya. Yang Li, and L. B. Lu, *Part. Part. Syst. Charact.* **30**, 630 (2013).
<https://doi.org/10.1002/ppsc.201300040>
21. E. Ozbay, *Science* (Washington, DC, U. S.) **311**, 189 (2006).
<https://doi.org/10.1126/science.1114849>
22. W. L. Liu, F. C. Lin, Y. C. Yang, C. H. Huang, S. Gwo, M. H. Huang, and J. Huang, *Nanoscale* **5**, 7953 (2013).
<https://doi.org/10.1039/C3NR02800C>
23. T. Wang, T. Tang, Y. Gao, Q. Chen, Zh. Zhang, and H. Bian, *Phys. E (Amsterdam, Neth.)* **112**, 128 (2019).
<https://doi.org/10.1016/j.physe.2018.10.033>
24. N. Fu, X. Ren, and J. X. Wan, *J. Nanomater.* **2019**, 8175803 (2019).
<https://doi.org/10.1155/2019/8175803>
25. E. Vasilaki, I. Georgaki, D. Vernardou, M. Vamvakaki, and N. Katsarakis, *J. Appl. Surf. Sci.* **353**, 865 (2015).
<https://doi.org/10.1016/j.apsusc.2015.07.056>
26. J. H. Lee, I. K. Kim, D. Cho, and H. J. Oh, *Carbon Lett.* **16**, 247 (2015).
<https://doi.org/10.5714/CL.2015.16.4.247>
27. H. Tian, Ch. Wan, X. Xue, X. Hu, and X. Wang, *Catalysts* **7**, 156 (2017).
<https://doi.org/10.3390/catal7050156>
28. W. Gao, M. Wang, Ch. Ran, X. Yao, H. Yang, J. Liu, D. He, and J. Bai, *Nanoscale* **6**, 5498 (2014).
<https://doi.org/10.1039/C3NR05466G>
29. D. A. Afanasyev, N. Kh. Ibrayev, T. M. Serikov, and A. K. Zeinidenov, *Russ. J. Phys. Chem. A* **90**, 833 (2016).
<https://doi.org/10.1134/S0036024416040026>
30. A. Zh. Zhumabekov, N. Kh. Ibrayev, and E. V. Seliverstova, *Theor. Exp. Chem.* **55**, 398 (2020).
<https://doi.org/10.1007/s11237-020-09632-8>
31. N. Ibrayev, A. Ishchenko, D. Afanasyev, and N. Zhumabay, *Appl. Phys. B* **125**, 182 (2019).
<https://doi.org/10.1007/s00340-019-7292-y>
32. V. Swamy, A. Kuznetsov, L. S. Dubrovinsky, R. A. Caruso, D. G. Shchukin, and B. C. Muddle, *Phys. Rev. B* **71**, 184302 (2005).
<https://doi.org/10.1103/PhysRevB.71.184302>
33. A. Jorio, R. Saito, G. Dresselhaus, and M. S. Dresselhaus, *Raman Spectroscopy in Graphene Related Systems* (Wiley-VCH, Berlin, 2011).
34. R. Kh. Dzhanabekova, E. V. Seliverstova, A. Zh. Zhumabekov, and N. Kh. Ibrayev, *Russ. J. Phys. Chem. A* **93**, 338 (2019).
<https://doi.org/10.1134/S0036024419020092>
35. R. Kh. Dzhanabekova, E. V. Seliverstova, and N. Kh. Ibrayev, *Russ. J. Phys. Chem. A* **91**, 1761 (2017).
<https://doi.org/10.1134/S003602441709028X>
36. A. Kokil, K. Yang, and J. Kumar, *J. Polym. Sci., Part B* **50**, 1130 (2012).
<https://doi.org/10.1002/polb.23103>
37. Sh. Li, D. Tao, Ya. Zhang, Y. Li, W. Yin, Q. Chen, and Z. Liu, *Nanophotonics* **8**, 899 (2019).
<https://doi.org/10.1515/nanoph-2019-0060>
38. A. de Sanctis, J. D. Mehew, M. F. Craciun, and S. Russo, *Materials* **11**, 1762 (2018).
<https://doi.org/10.3390/ma11091762>
39. V. Patil, A. Capone, S. Strauf, and E. H. Yang, *Sci. Rep.* **3**, 2791 (2013).
<https://doi.org/10.1038/srep02791>
40. T. He, Y. Zhao, X. Zhang, W. Lin, K. Fu, C. Sun, F. Shi, X. Ding, G. Yu, K. Zhang, Sh. Lu, X. Zhang, and B. Zhang, *Nanophotonics* **7**, 1557 (2018).
<https://doi.org/10.1515/nanoph-2018-0061>
41. X. Kong, C. Liu, W. Dong, X. Zhang, Ch. Tao, L. Shen, L. Zhou, Y. Fei, and Sh. Ruan, *Appl. Phys. Lett.* **94**, 123502 (2009).
<https://doi.org/10.1063/1.3103288>
42. H. Ahmad, M. Tajdidzadeh, K. Thambiratnam, and M. Yasin, *Laser Phys.* **28**, 066204 (2018).
<https://doi.org/10.1088/1555-6611/aab451>
43. S. Thomas, E. H. M. Sakho, N. Kalarikkal, O. S. Oluwafemi, and J. Wu, *Nanomaterials for Solar Cell Applications* (Elsevier, Amsterdam, 2019).
44. K. S. Novoselov, A. K. Geim, S. V. Morozov, D. Jiang, Y. Zhang, S. V. Dubonos, I. V. Grigorieva, and A. A. Firsov, *Science* (Washington, DC, U. S.) **306**, 666 (2004).
<https://doi.org/10.1126/science.1102896>
45. R. Maiti, T. K. Sinha, S. Mukherjee, B. Adhikari, and S. K. Ray, *Plasmonics* **11**, 1297 (2016).
<https://doi.org/10.1007/s11468-015-0175-0>
46. Y. Liu, R. Cheng, L. Liao, H. Zhou, J. Bai, G. Liu, L. Liu, Y. Huang, and X. Duan, *Nat. Commun.* **2**, 579 (2011).
<https://doi.org/10.1038/ncomms1589>
47. T. J. Echtermeyer, L. Britnell, P. K. Jasnós, A. Lombardo, R. V. Gorbachev, A. N. Grigorenko, A. K. Geim, A. C. Ferrari, and K. S. Novoselov, *Nat. Commun.* **2**, 458 (2011).
<https://doi.org/10.1038/ncomms1464>

Translated by O. Kadkin